**Supplemental Figure 1.**

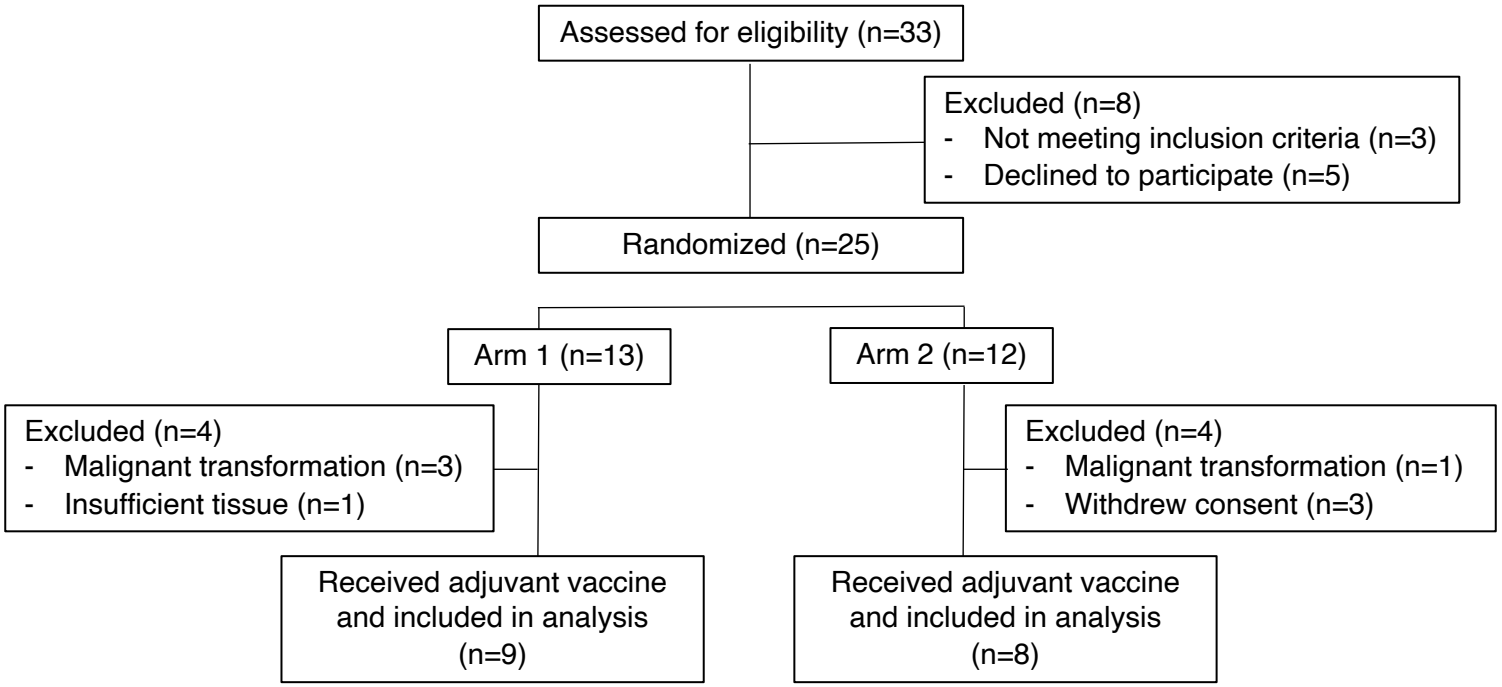


**Supplemental Figure 1. The flow diagram of this study.**

## Supplemental Figure 2.

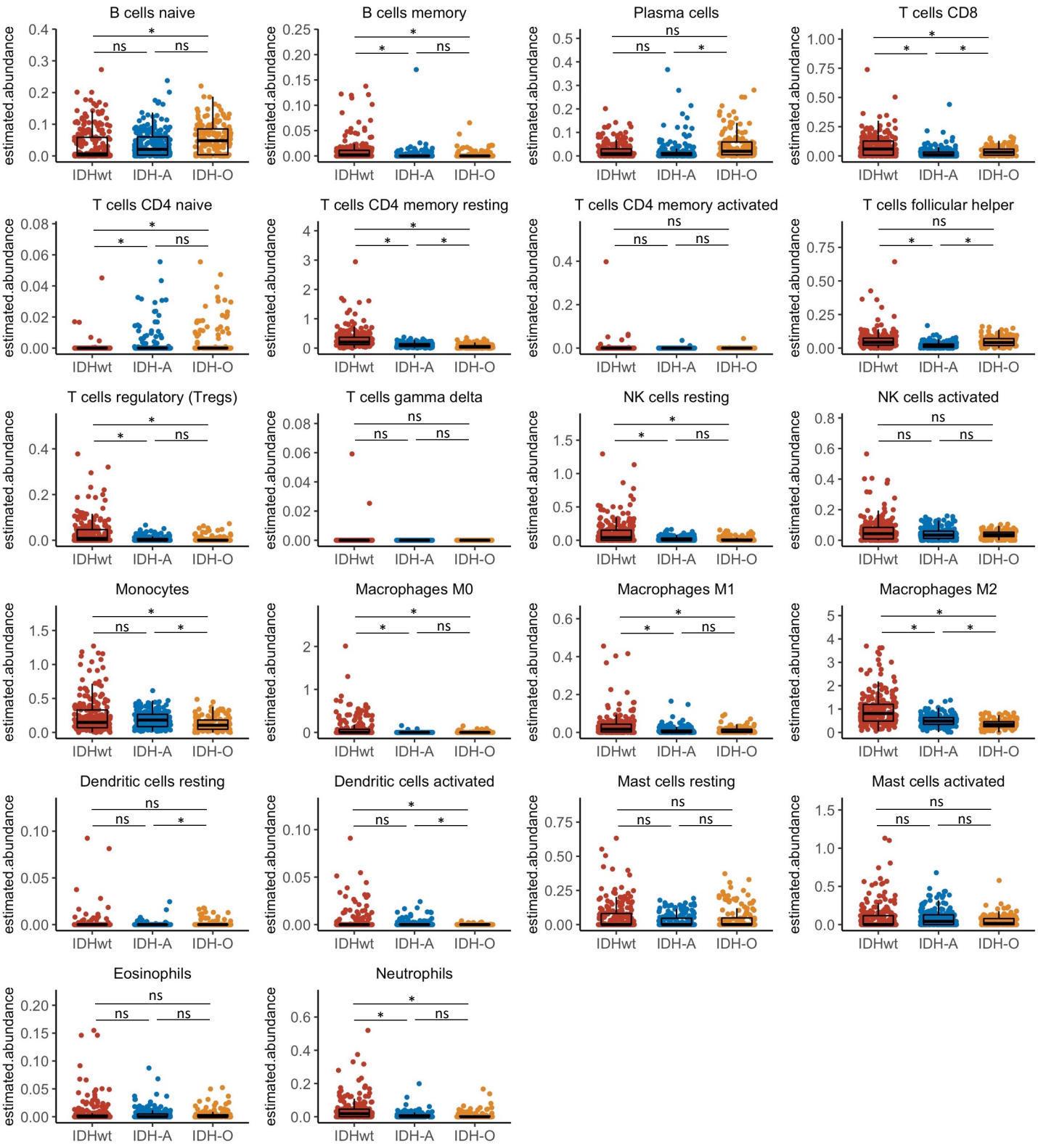


**Supplemental Figure 2. Astrocytoma and oligodendroglioma have similar immune cell compositions in their tumor microenvironment.** Bulk RNA-seq gene expression data of IDH-wildtype glioma (IDHwt), IDH mutant, 1p19q-non-codeleted astrocytoma (IDH-A), and IDH-mutant, 1p19q-codeleted oligodendroglioma (IDH-O) from TCGA were downloaded through the UCSC Xena Toil web portal, and analyzed by CIBERSORTx deconvolution. Although slight differences were observed for the densities of some immune cells between IDH-A and IDH-O, the differences were much more remarkable between IDHwt and IDH-mutant glioma. ns; non-significant, *$p$<0.05 (calculated by Kruskal-Wallis test with Holm's multiple testing corrections followed by the Dunn post hoc test ).

## Supplemental Figure 3.

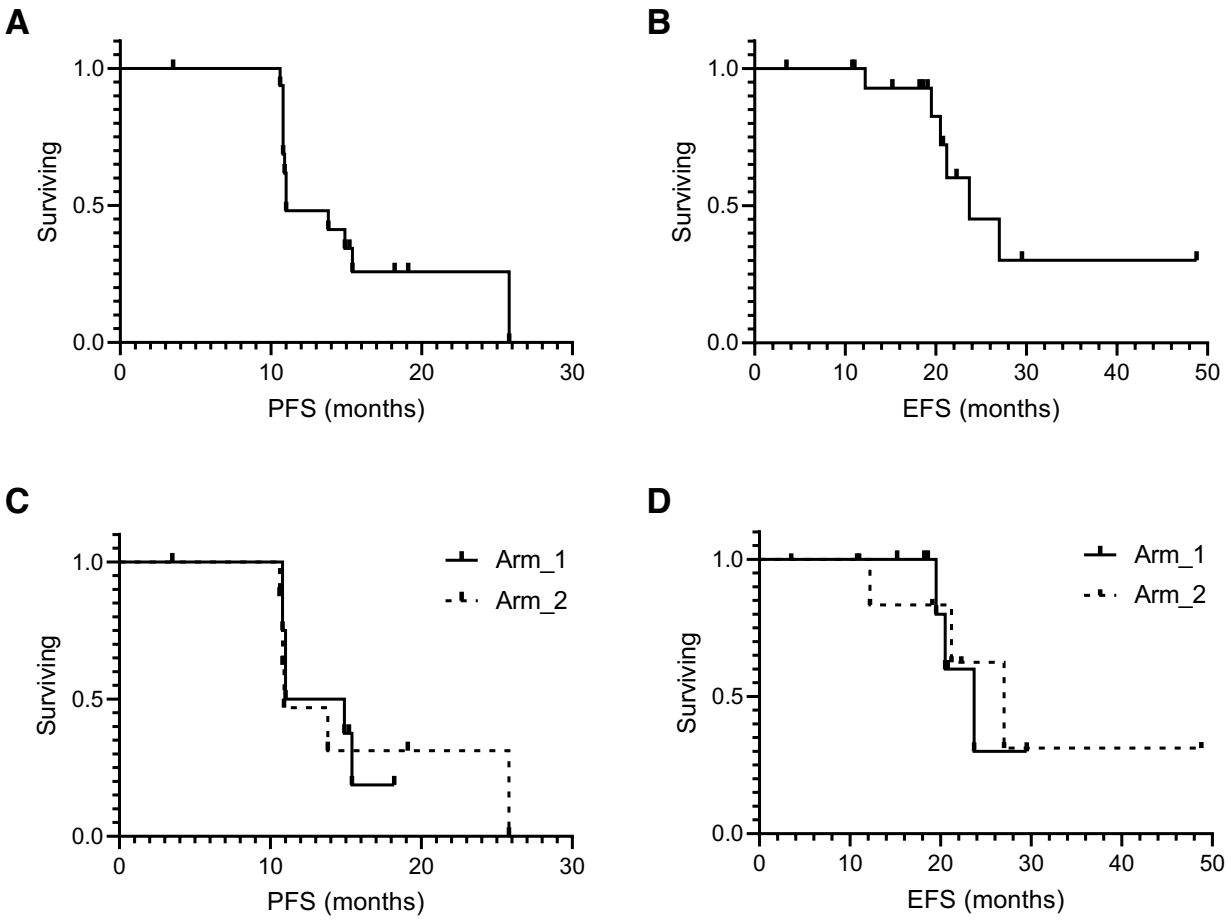


**Supplemental Figure 3. Clinical outcomes of the patients in this study. (A)** Progression free survival (PFS) was calculated from time of post-operative A1 vaccine to time of centrally confirmed imaging progression. Median PFS was 11.0 months (95% CI 10.8 – 15.4 months). **(B)** Event free survival (EFS) was calculated from time of post-operative A1 vaccine to time of new therapy. Median EFS was 23.7 months (95% CI 19.5 months – not reached). **(C, D)** There were no significant differences between PFS or EFS between Arms.

## Supplemental Figure 4.

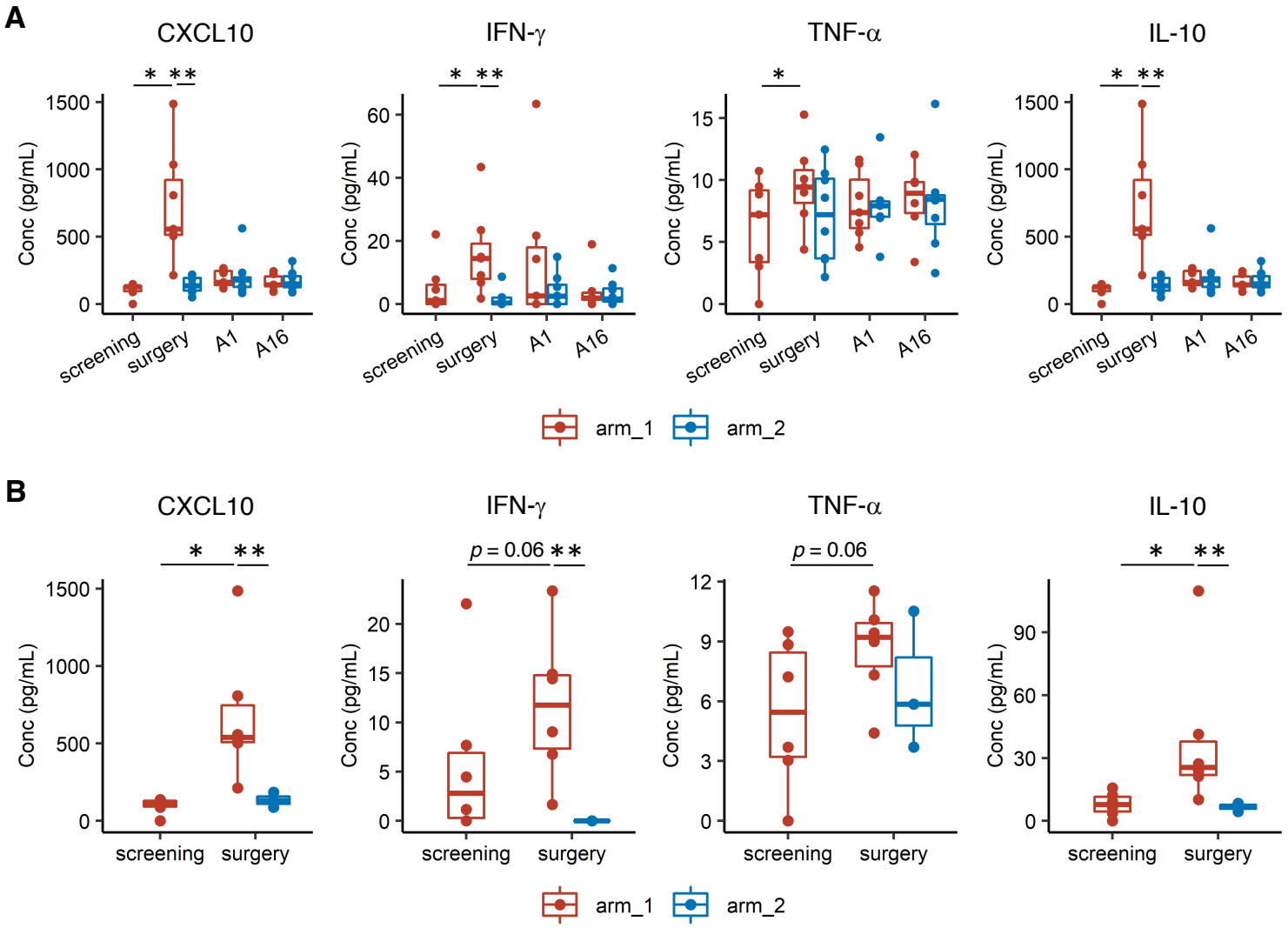


**Supplemental Figure 4 (related to the data set in Figure 2). Upregulation of type-1 chemokines and cytokines induced by neoadjuvant vaccination was observed in Arm 1. (A)** Serum concentrations of multiple chemokines and cytokines were measured by Luminex multiplex assay. The concentrations of type-1 chemokines and cytokines, such as CXCL10, IFN-γ, TNF-α, and IL-10, were elevated in Arm 1 samples on the day of surgery. On the other hand, none of them were upregulated in both arms on A16 date which are at three weeks after the most recent prior vaccination. **(B)** The same trends were observed when oligodendroglioma patients were selectively analyzed, though statistically significant differences in IFN-γ and TNF-α between the baseline and day of surgery in Arm 1 were lost because of the smaller number of cases. *$p$<0.05 (calculated by paired Wilcoxon test) and **$p$<0.05 (calculated by non-paired Wilcoxon test).

**Supplemental Figure 5.**

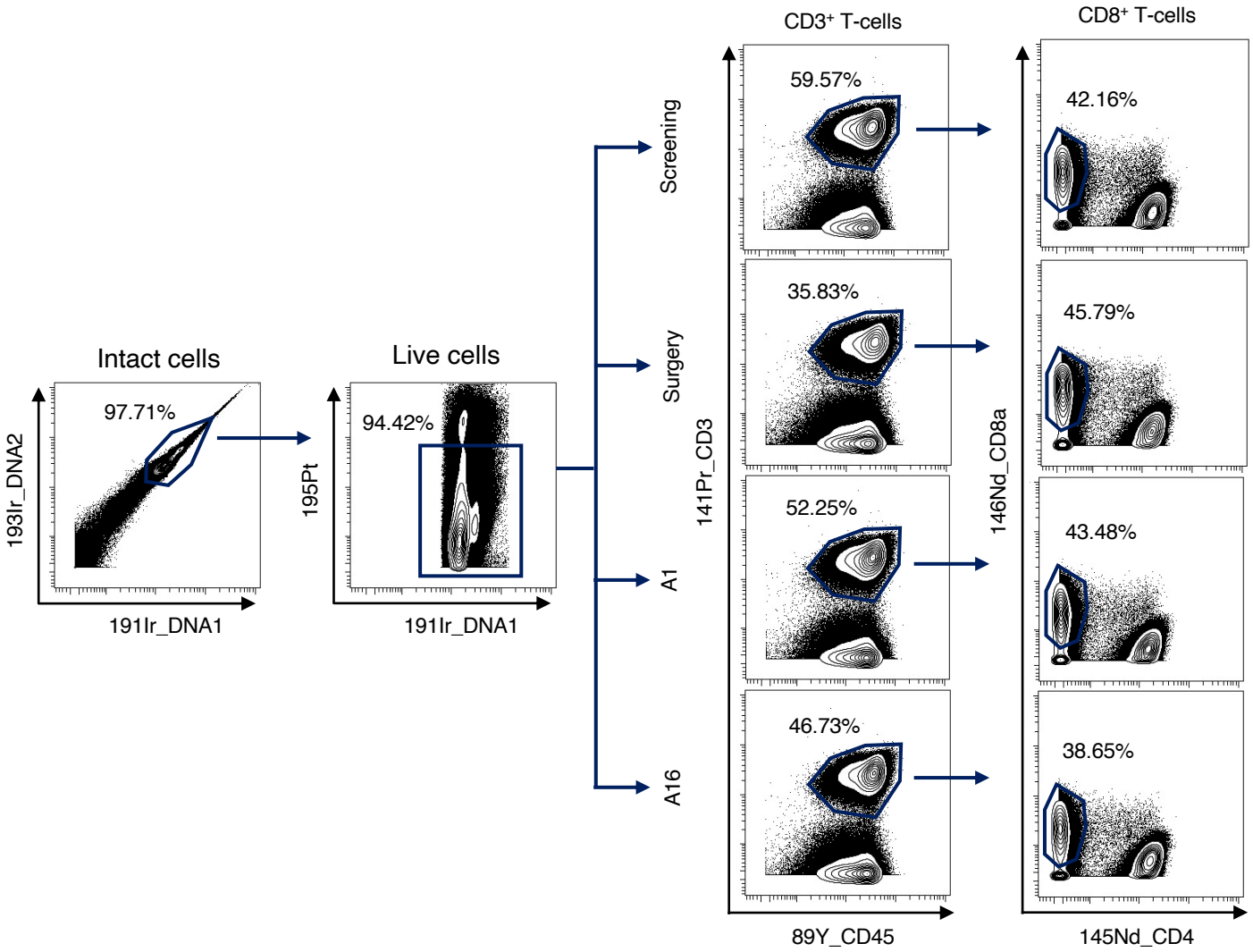


**Supplemental Figure 5 (related to the data set in Figure 3). Gating strategy for CD8⁺ T-cells from PBMC on mass cytometric analyses.** A representative gating strategy to identify CD8⁺ T-cells from PBMCs derived from one patient. Cells staining double-positive with iridium (Ir) intercalator in channels 191 and 193 were identified as intact cells (left). Cells with low cisplatin staining were identified as live cells (second to left). Cells were then debarcoded based on their three-metal combinations from barcoding reagents, and divided into samples from each time point. Cells staining positive for CD45 and CD3 were selected as T-cells (second to right), and positive for CD8a were identified as CD8⁺ T-cells (right).

## Supplemental Figure 6.

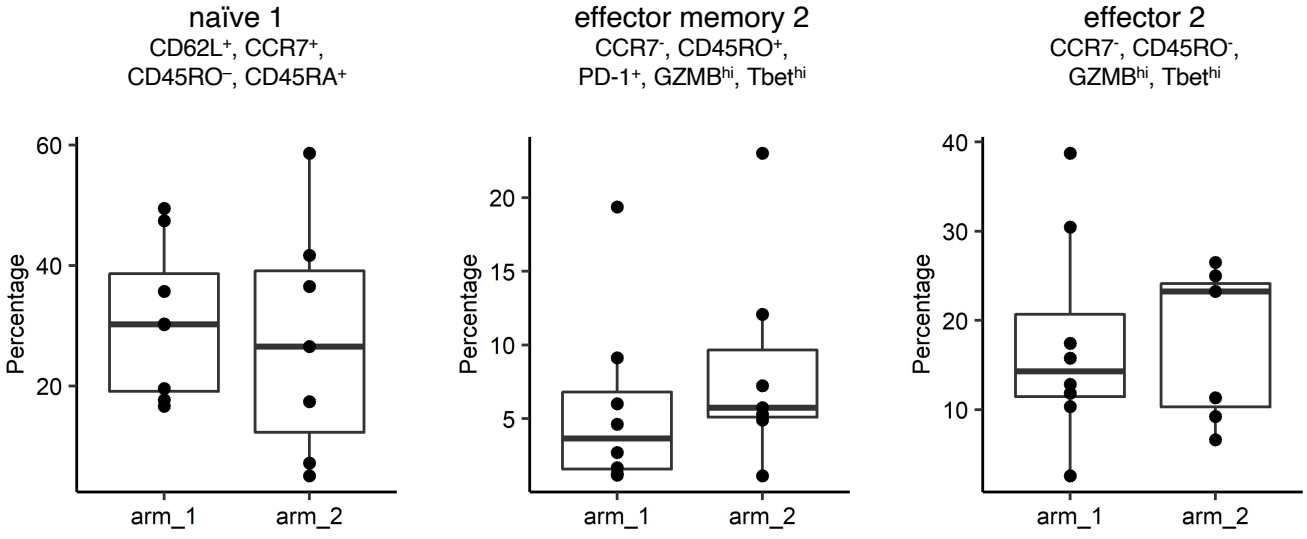


**Supplemental Figure 6 (related to the data set in Figure 3). No differences in the cluster proportions were observed between Arm 1 and Arm 2 peripheral CD8+ T-cell samples on the day of surgery.** In the mass cytometric analyses using peripheral CD8+ T-cells, the proportions of the clusters, which were significantly downregulated (naïve) or upregulated (PD-1+ GZMBhi Tbethi effector memory and GZMBhi Tbethi effector) by neoadjuvant vaccination in Arm 1 samples, were found insignificantly different between Arms 1 and 2 samples on the day of surgery.

## Supplemental Figure 7.

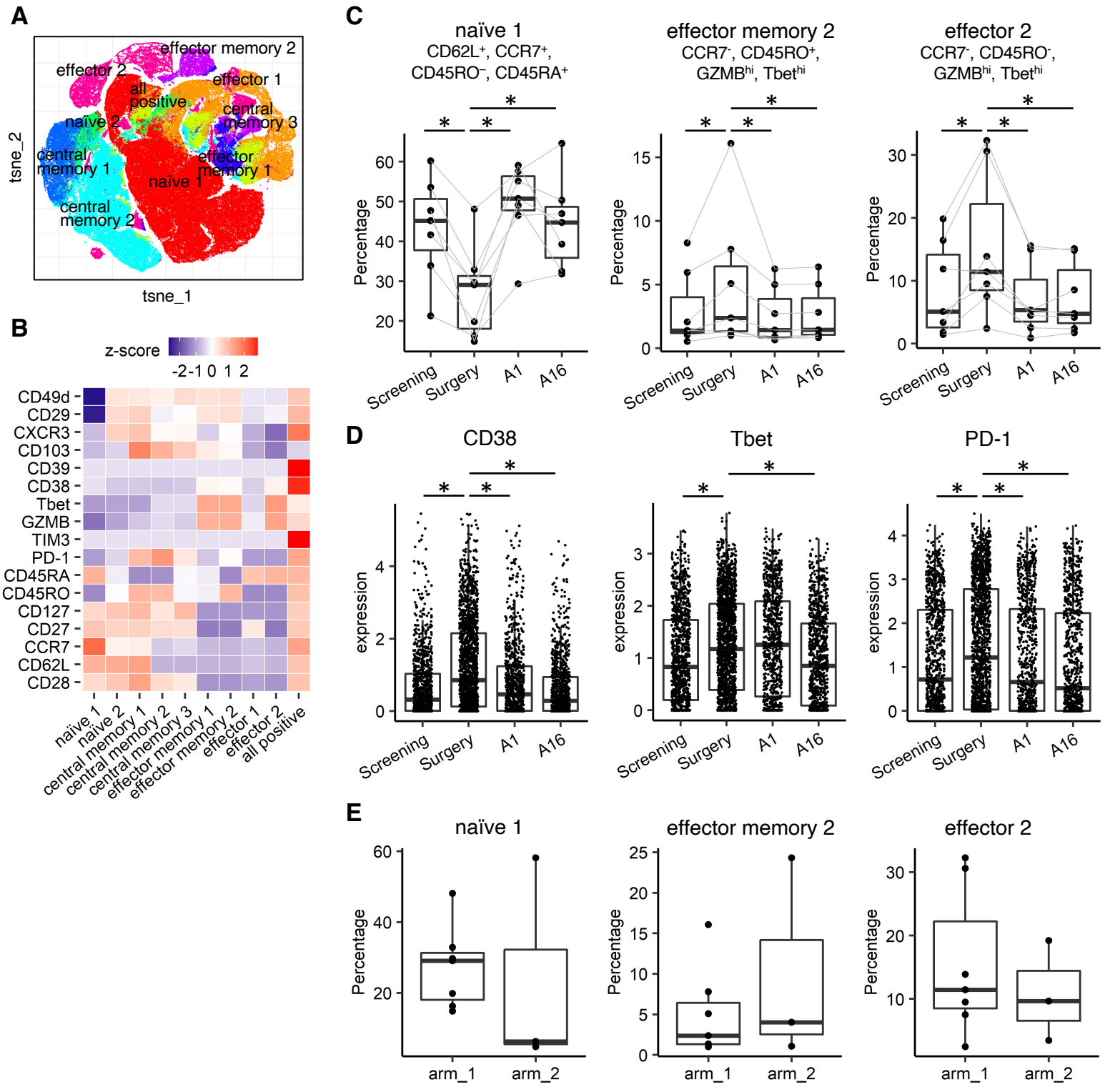


**Supplemental Figure 7 (related to the data set in Figure 3). The same trends were observed in the dataset from only oligodendroglioma patients in mass cytometric analyses using PBMC.** The mass cytometry dataset from oligodendroglioma patients (seven in Arm 1 and three in Arm 2) were selectively analyzed to evaluate the influence of the bias of tumor histology. **(A)** $CD8^+$ T-cells were subjected to t-SNE for visualization and clustered by FlowSOM. **(B)** Heatmap visualizing the relative expression (Z score) of T-cell-relevant markers in each subpopulation. **(C)** Neoadjuvant vaccine with GBM6-AD and poly-ICLC increases $GZMB^{hi}$ $Tbet^{hi}$ effector memory and $GZMB^{hi}$ $Tbet^{hi}$ effector $CD8^+$ T-cells while decreasing naïve $CD8^+$ T-cells in Arm 1 patients. *$p<0.05$ (paired Wilcoxon test). **(D)** The expression of activation markers on every single cell in this $GZMB^{hi}$ $Tbet^{hi}$ effector memory cluster were enhanced in the post-neoadjuvant vaccinated samples. *$p<0.05$ (non-paired t-test). **(E)** No differences in the proportions of each cluster between Arm 1 and Arm 2 samples were seen on the day of surgery.

## Supplemental Figure 8.

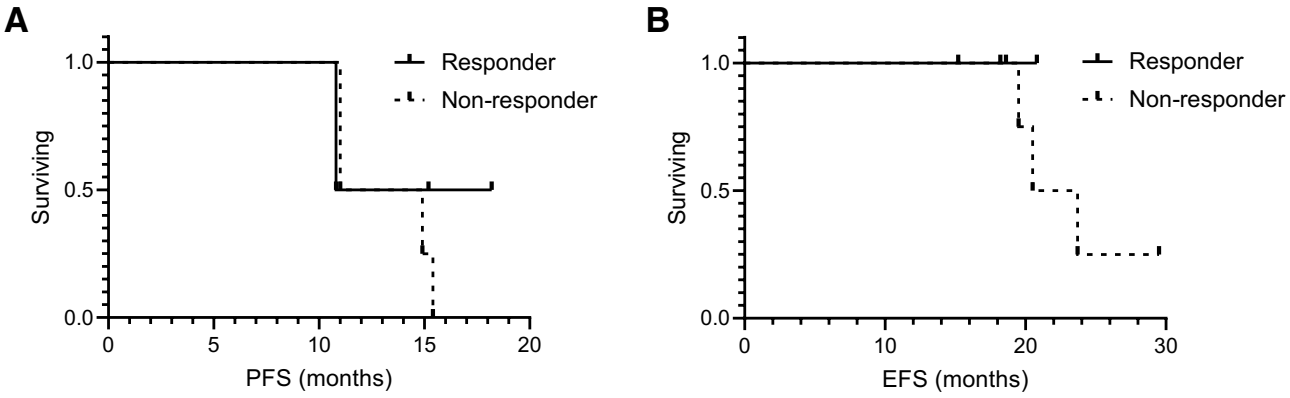


**Supplemental Figure 8. The comparison of clinical outcomes between immunological responders and non-responders.** Four patients who demonstrated a 10% or higher increase in the proportion of either PD-1$^{+}$ GZMB$^{hi}$ Tbet$^{hi}$ effector memory or GZMB$^{hi}$ Tbet$^{hi}$ effector population following the neoadjuvant vaccination in peripheral blood, determined by CyTOF analyses, were defined as immunological responders (103-018, -026, -029, -051). There were not clear associations between the immunological response and (A) PFS or (B) EFS.

## Supplemental Figure 9.

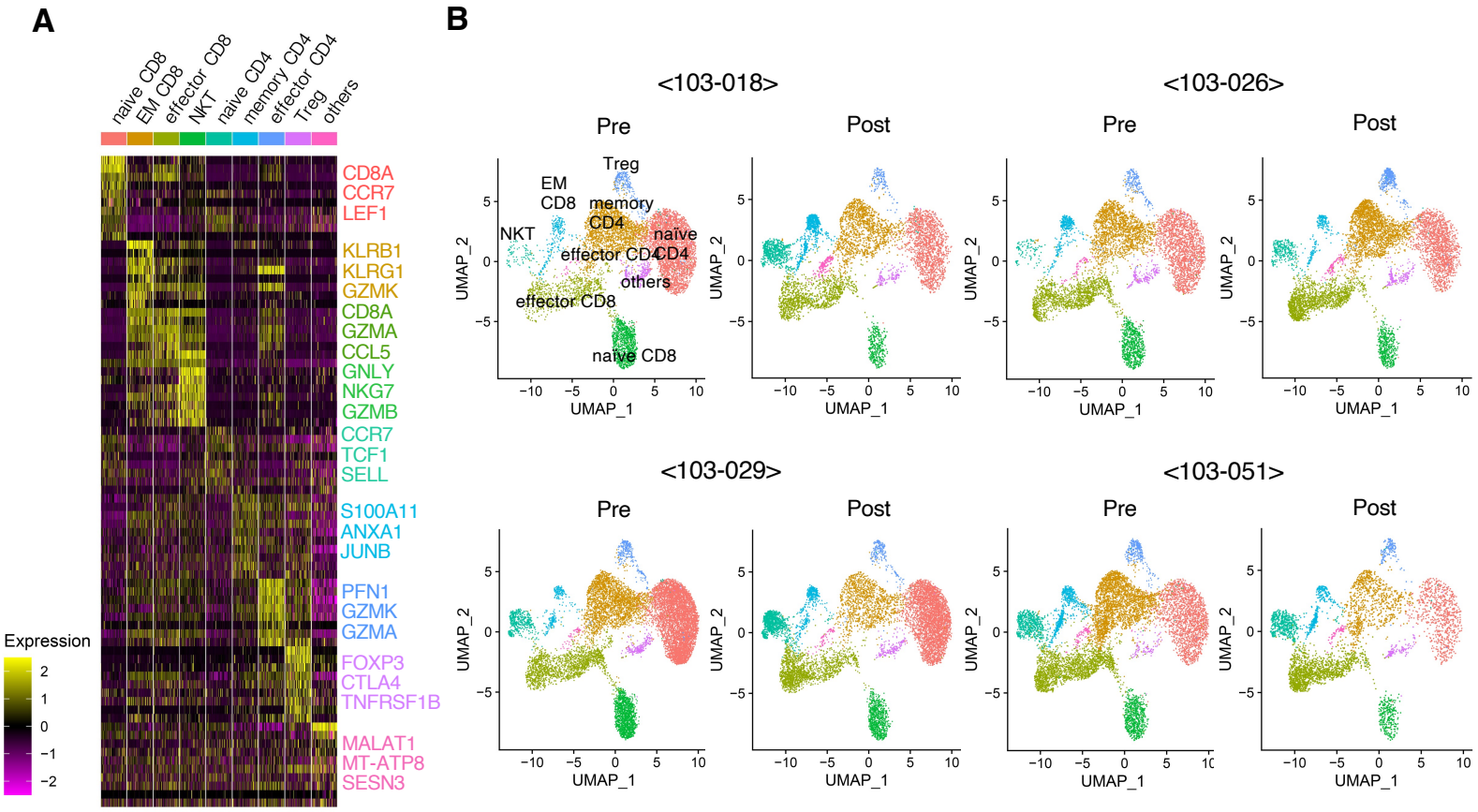


**Supplemental Figure 9 (related to the data set in Figure 4). ScRNA-seq analyses showed the increases of effector CD4⁺ and CD8⁺, and decreases of naïve CD4⁺ and CD8⁺ T-cell populations in post-neoadjuvant samples.** ScRNA-seq and scTCR-seq analyses were conducted using pre- and post-neoadjuvant vaccinated PBMCs from the four immunological responders, defined based on mass cytometric analysis (103-018, -26, -29, -51), on 10x GENOMICS platform. T- and NKT-cell populations were extracted from the original dataset, and re-clustered and grouped into nine subpopulations. **(A)** Heat map of differentially expressed genes between cells belonging to different T-cell subsets. Specific genes that are associated with different T-cell clusters are highlighted. **(B)** UMAP of T- and NKT-cells present in PBMC samples in each sample. The proportion of effector CD8⁺ T-cells and NKT-cells demonstrated a trend toward an increase in post-neoadjuvant vaccinated samples.

## Supplemental Figure 10.

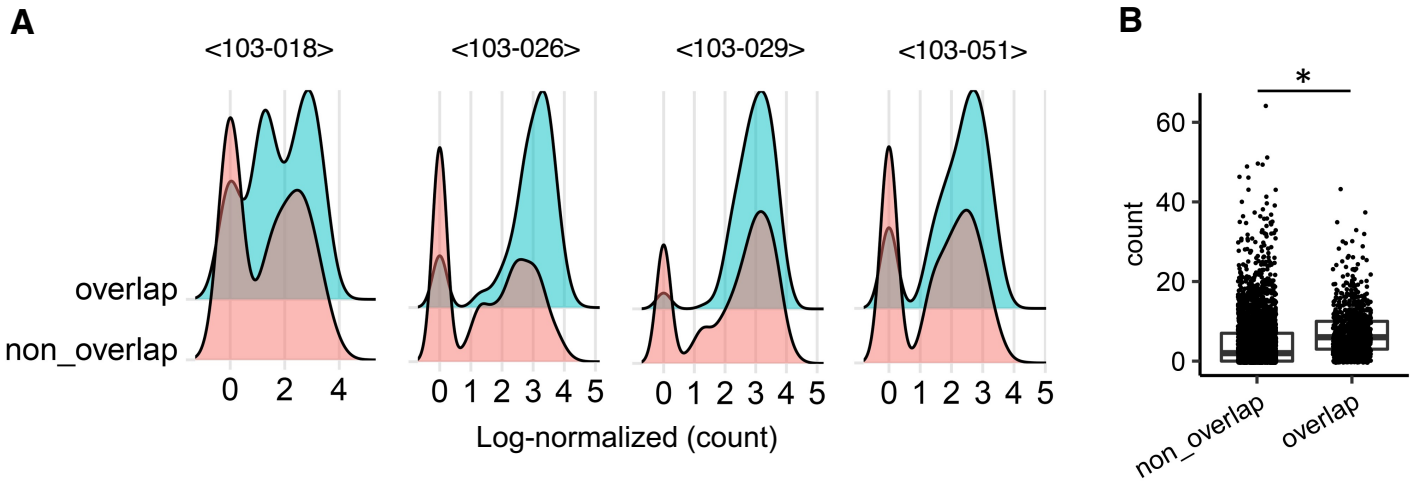


**Supplemental Figure 10 (related to the data set in Figure 5). The upregulation of GZMB was more remarkable in the effector CD8⁺ T-cells that existed in both PBMC and the tumor than in the effector CD8⁺ T-cells that were enriched in PBMC but not found in the tumor.** Within the effector CD8 cluster, the T-cells with overlapped clonotypes expressed a higher level of GZMB than other T-cells. Log-normalized (count) on x-axis was calculated as log (count / [total count of the cell] x 10,000 + 1). *p<0.05 (non-paired t-test).

**Supplemental Figure 11.**

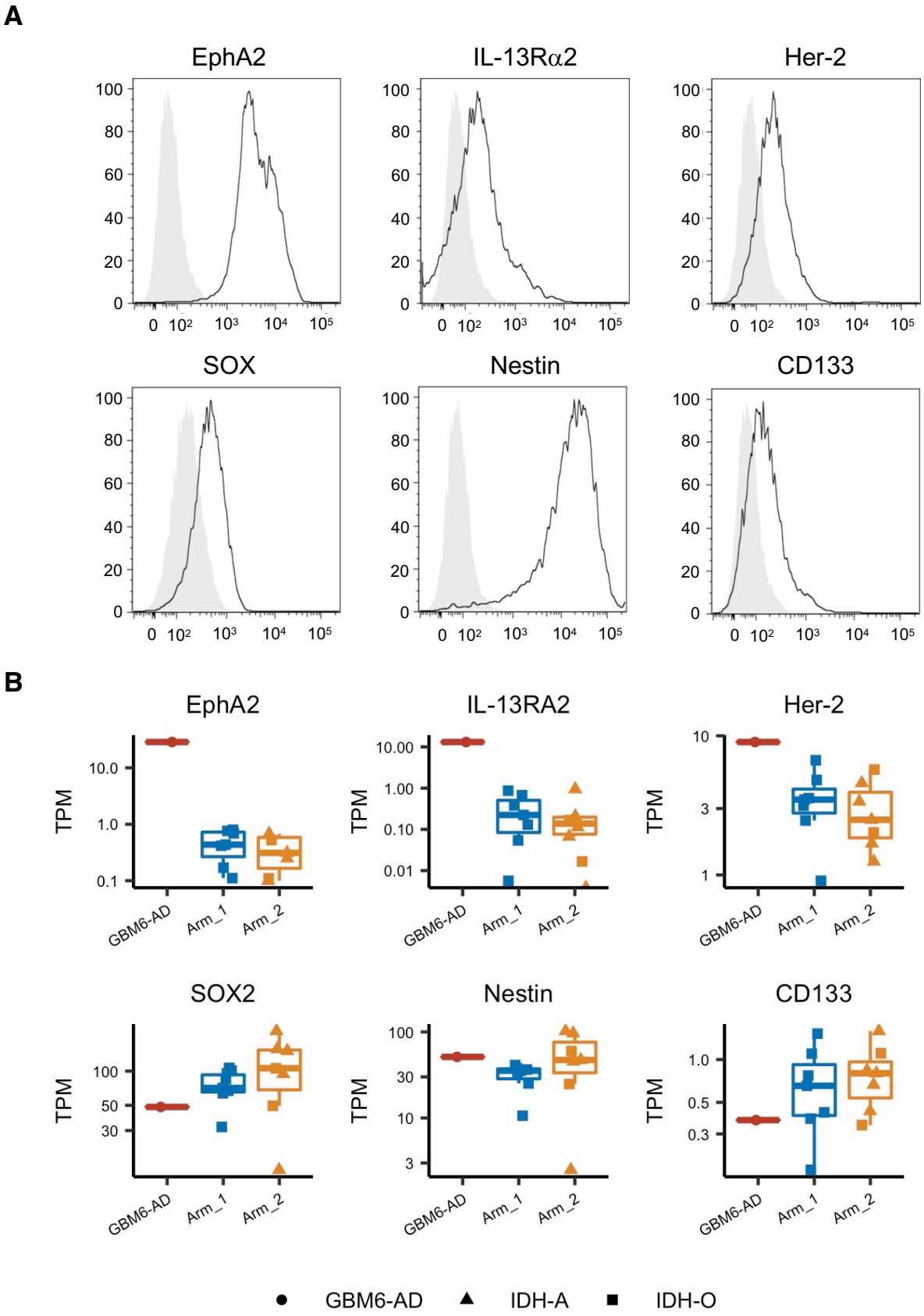


**Supplemental Figure 11. The expression of glioma associate antigens (GAAs) or stem cell markers in GBM6-AD cells or tumor specimens. (A)** Flow cytometry analyses demonstrated that GBM6-AD cells express not only several GAAs, such as EphA2, IL-13Rα2, and Her-2, but also several brain tumor initiating cells (BITCs) markers, such as SOX, Nestin and CD133. (B) Bulk RNA-seq analysis also demonstrated that both GBM6-AD and IDH-mutant LGG tumors express these antigens, albeit at different levels.

## Supplemental Figure 12.

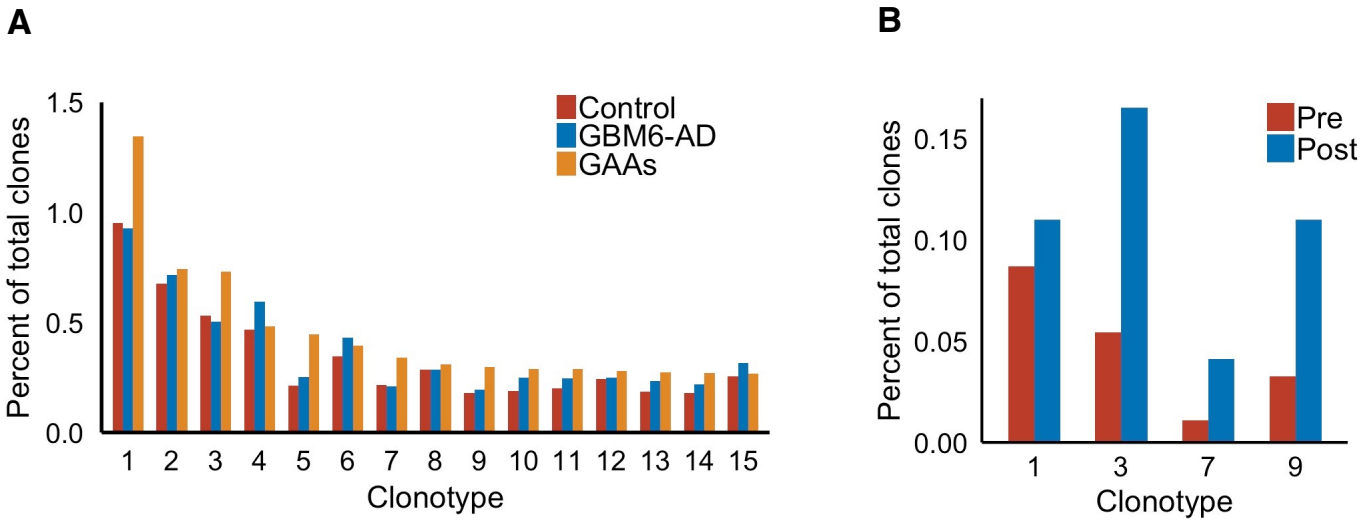


**Supplemental Figure 12. Some of the TCR clones responded to the GBM6-AD lysate-derived antigens. (A)** In patient 103-018, four of the top 15 most abundant $CD8^+$ T-cell-derived TCR clonotypes (i.e. clones 1, 3, 7, and 9) enriched more than 20% in response to GAA-stimulation when compared with the control group with no stimulation. However, a robust response of these TCR clones to GBM6-AD was not observed. **(B)** Nevertheless, scTCR-seq analyses showed that the frequencies of these four $CD8^+$ T-cell clones among total T-cells in peripheral blood increased following the vaccination of GBM6-AD in this patient.

## Supplemental Figure 13.

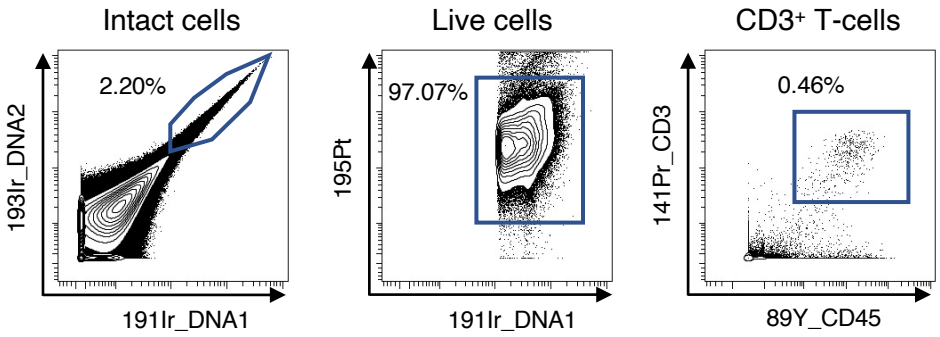


**Supplemental Figure 13 (related to the data set in Figure 6). Gating strategy for mass cytometric analyses of CD3⁺ T-cells dissociated from tumor samples.** A representative gating strategy to identify CD3⁺ T-cells from single-cell suspensions obtained from the tumor of one patient. These samples were not barcoded and stained independently. Cells staining double-positive with iridium (Ir) intercalator in channels 191 and 193 were identified as intact cells (left). Cells with low cisplatin staining were identified as live cells (middle). Cells staining positive for CD45 and CD3 were selected as CD3⁺ T-cells (right).

## Supplemental Figure 14.

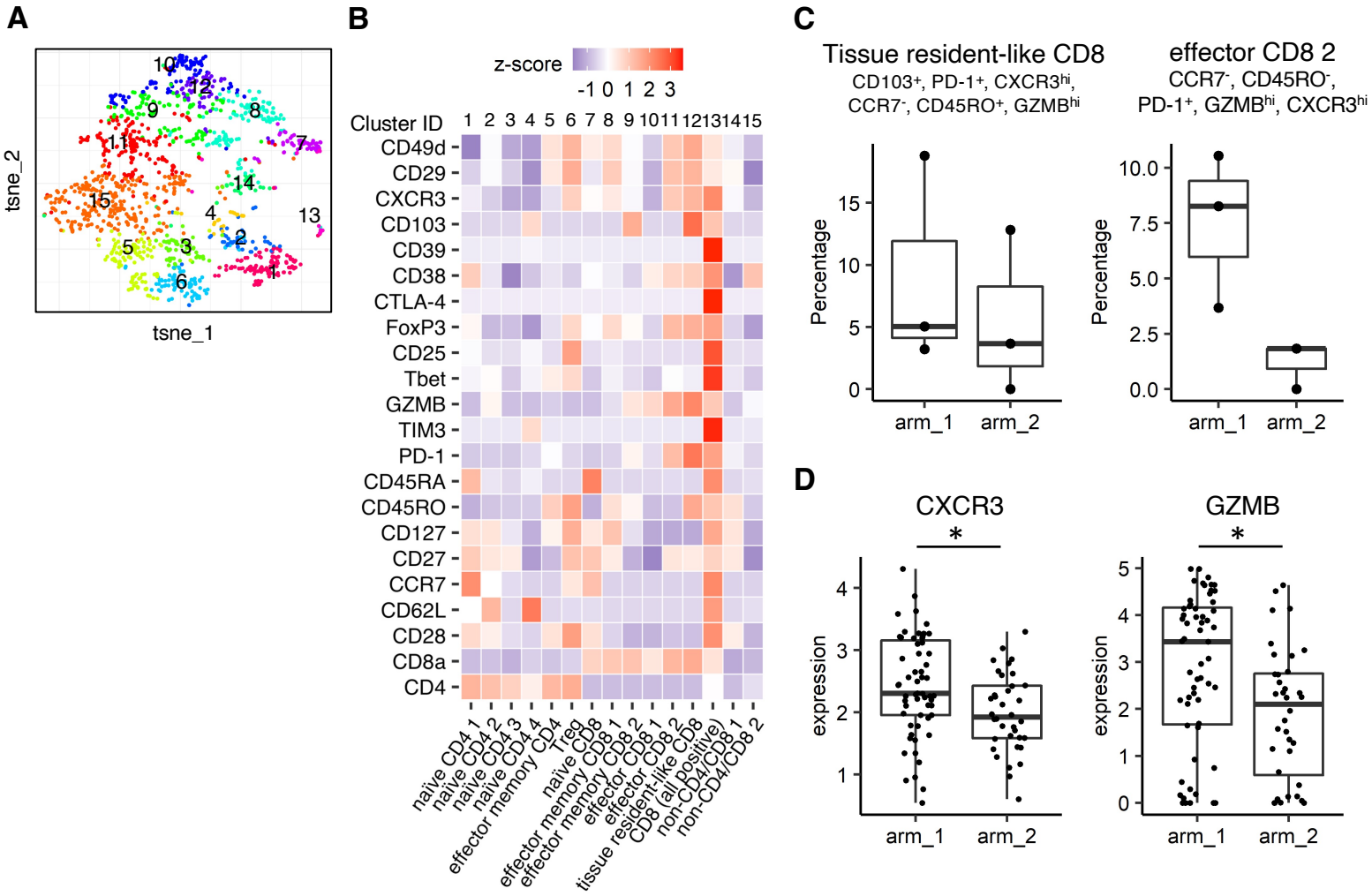


**Supplemental Figure 14 (related to the data set in Figure 6). The same trends were observed in the mass cytometric analyses of tumor-infiltrating leukocytes when selected for oligodendroglioma patients only.** The mass cytometry dataset from oligodendroglioma patients (three patients in each arm) was selectively analyzed for the potential bias of tumor histology. **(A)** CD3+ T-cells were subjected to t-SNE and clustered by FlowSOM. **(B)** Heatmap visualizing the relative expression (Z score) of T-cell-relevant markers in each subpopulation. **(C)** The proportion of tissue resident-like CD8+ T-cells with effector memory phenotype (CD103+, PD-1+, CXCR3hi, CCR7-, CD45RO+, GZMBhi) and effector CD8+ T-cells showed a trend toward an increase in Arm 1 samples but without statistical significance. **(D)** TILs in this of tissue resident-like CD8+ T-cells cluster in Arm 1 tumors demonstrated significantly higher expression levels for the CXCR3 and GZMB than those in Arm 2 tumors.

## Supplemental Figure 15.

**A**

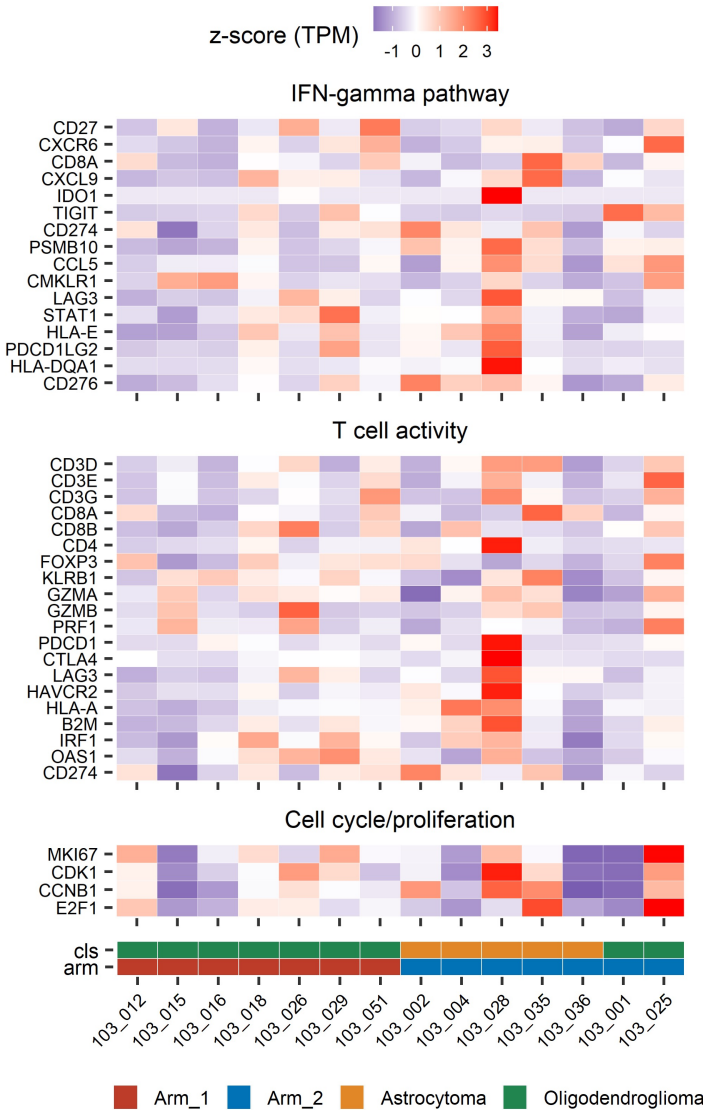


**Supplemental Figure 15. The differences in the expression of immune-related genes between Arm 1 and Arm 2 tumors were not detected in bulk RNA-seq analyses.** Bulk RNA-seq analysis using surgically resected tumor specimens was performed to evaluate the immune profile of TIL. However, the heat map, based on the relative TPM values of each immune related signature genes, didn't show any differences in the expression patterns of these genes between Arm 1 and Arm 2 tumors.

Supplemental Table 1. Antibodies panel for mass cytometric analysis.

| Label | Target | Clone | Vender | Cat # |
|---|---|---|---|---|
| 89Y | CD45 | HI30 | Fludigm | 3089003B |
| 141Pr | CD3 | UCHT1 | Fludigm | 3141019B |
| 142Nd | CD19 | HIB19 | Fludigm | 3142001B |
| 143Nd | CD45RA | HI100 | Fludigm | 3143006B |
| 144Nd | CD11b | ICRF44 | Fludigm | 3144001B |
| 145Nd | CD4 | RPA-T4 | Fludigm | 3145001B |
| 146Nd | CD8 | RPA-T8 | Fludigm | 3146001B |
| 147Sm | CD11c | Bu15 | Fludigm | 3147008B |
| 148Nd | CD14 | RMO52 | Fludigm | 3148010B |
| 149Sm | CD127 | A019D5 | Fludigm | 3149011B |
| 150Nd | CD86 | IT2.2 | Fludigm | 3150020B |
| 151Eu | CD103 | Ber-ACT18 | Fludigm | 3151011B |
| 152Sm | HLA-DR | L243 | BioLegend | 307651 |
| 153Eu | CD62L | DREG-56 | Fludigm | 3153004B |
| 154Sm | TIM3 | F38-2E2 | Fludigm | 3154010B |
| 155Gd | PD-1 | EH12.2H7 | Fludigm | 3155009B |
| 156Gd | CD29 | TS2/16 | Fludigm | 3156007B |
| 157Gd | CXCR3 | G025H7 | BioLegend | 353733 |
| 158Gd | CD27 | L128 | Fludigm | 3158010B |
| 159Tb | CX3CR1 | 2A9-1 | BioLegend | 341602 |
| 160Gd | CD28 | CD28.2 | Fludigm | 3160003B |
| 161Dy | Tbet | 4B10 | Fludigm | 3161014B |
| 162Dy | FoxP3 | PCH101 | Fludigm | 3162011A |
| | | 259D/C7 | Fludigm | 3162024A |
| 163Dy | CD33 | WM53 | Fludigm | 3163023B |
| 164Dy | CD45RO | UCHL1 | Fludigm | 3164007B |
| 165Ho | CD163 | GHI/61 | Fludigm | 3165017B |
| 166Er | CD39 | A1 | BioLegend | 328221 |
| 167Er | CCR7 | G043H7 | Fludigm | 3167009A |
| 168Er | CD206 | 15-2 | Fludigm | 3168008B |
| 169Tm | CD25 | 2A3 | Fludigm | 3169003B |
| 170Er | CTLA-4 | 14D3 | Fludigm | 3170005B |
| 171Yb | CD68 | Y1/82A | Fludigm | 3171011B |
| 172Yb | CD38 | HIT2 | Fludigm | 3172007B |

| | | | | |
|---|---|---|---|---|
| 173Yb | GZMB | GB11 | Fludigm | 3173006B |
| 174Yb | CD49d | 9F10 | Fludigm | 3174018B |
| 175Lu | PD-L1 | 29E.2A3 | Fludigm | 3175017B |
| 176Yb | CD56 | NCAM16.2 | Fludigm | 3176008B |
| 209Bi | CD16 | 3G8 | Fludigm | 3209002B |